ELSEVIER

Cement and Concrete Composites **19** (1997) 45–57

0958-9465/97/$17.00+0.00

PII:S0958-9465(96)00042-X

Distributed Fiber Bragg Grating Strain Sensing in Reinforced Concrete Structural Components

M. A. Davis,[a] D. G. Bellemore[b] & A. D. Kersey,[a]

[a]Code 5673, Naval Research Laboratory, Washington, DC 20375, USA
[b]SFA Inc., Landover, 20 785, MD, USA

Abstract

Fiber Bragg grating sensors are of particular interest for distributed sensor applications, where gratings can be addressed using time- and wavelength-division techniques to provide the strain distribution along a structural component. This paper describes the use of a prototype Bragg grating instrumentation system for monitoring the strain at several locations through reinforced concrete beams and decks which are tested to failure. Strain readings are obtained from a number of multiplexed sensors which are bonded to the rebar reinforcement, free floating in the concrete, and embedded in composite materials attached to the concrete. © 1997 Elsevier Science Limited

Keywords: Fiber Bragg grating, fiber optics, strain sensor.

INTRODUCTION

Considerable research activity has been centered lately on the development of 'smart structures'; i.e. structures that have the capability to provide real-time information on their health and integrity and possibly adapt to compensate for any anomalous in-service or environmental loading, or other potentially structural-weakening conditions. The first step in the development of this technology is to incorporate a level of structural sensing capability. This can be achieved, for example, through the use of strain measurements taken at multiple locations throughout the structure. Many issues need to be addressed in the implementation of this technology—such as the compatibility of the sensing systems with the fabrication processes, incorporation of a telemetry means for reading multiple strain gages, and material–sensor interactions, such as would occur due to the corrosive nature of certain materials, for example—and many groups world-wide are focusing on these aspects.

Within the smart structures community there has been increasing recognition of the potential of fiber-optic sensors,[1–3] particularly fiber Bragg grating sensors, for multi-point structural strain monitoring. These sensors posses a number of unique advantages compared with their conventional counterparts, including immunity to electromagnetic interference, absolute strain sensing capability, ease of multiplexing,[4] and compatibility with being embedded in a range of structural materials. Fiber Bragg gratings are intrinsic, 'spectrally encoded' sensors; the strain information from a grating is encoded onto the wavelength reflected by the device. This enables a grating sensor to tolerate changes in the optical losses of the system or fluctuations in the source power level. The wavelength-encoded nature of the output also provides the basis for the multiplexing of several gratings along a single optical fiber. As the gratings can be written at different initial wavelengths, they can be identified by their spectral location, and correlated to physical locations along the fiber. This gives the sensor system the capability to 'map' the strain along the fiber, and offers a new and very powerful sensing capability for structural analysis.

The demodulation, or decoding, of the information provided by these sensors is achieved by monitoring the often small wavelength shifts in the optical signal returned by the device. Several different techniques have been developed to achieve this including frequency-

dependent filters,[5] interferometers[6,7] and some active laser configurations.[8] A tunable narrowband filter is a device that can be used to monitor the signals from several multiplexed fiber Bragg grating (FBG) sensors, as was first demonstrated by Kersey *et al.*[9] This demodulation concept [a fiber-coupled Fabry–Perot (FFP)] is the basis of the prototype Bragg grating instrumentation system described in this work.

This paper describes the results obtained when multiple FBG sensors were embedded in reinforced concrete beams and loaded until failure. A detailed description is also given of the prototype instrumentation system which was originally designed to monitor arrays of up to four FBG sensors but has been expanded to accommodate 12 devices on a single fiber.

BACKGROUND

Hill *et al.*[10] first discovered the UV photosensitivity of germanium-doped optical fiber and demonstrated the possibility of an intra-core fiber Bragg grating. However, the development of a side holographic exposure technique to produce FBGs[11] and grating production on-line as the optical fiber is drawn[12] have refined the FBG manufacturing technique so that the devices are readily available and reproducible. FBGs are created by forming a small periodic modulation of the refractive index of the core of an optical fiber, with usually an index variation of only between 10^{-5} to 10^{-3}. To create this index change the core of the fiber is exposed to a periodic spatially varying UV source. The two predominant techniques used to achieve this condition are the interference pattern created by two UV beams, and one UV beam focused through a phase mask.[13] The period of the modulation (λ) in the index of refraction of the fiber's core is given by:

$$\lambda = \frac{\lambda_{UV}}{2\sin(\theta/2)} \tag{1}$$

where λ_{UV} is the wavelength of the UV source, and θ is the angle between the two interfering UV beams. For Ge-doped optical fibers, UV wavelengths of 248 nm and 193 nm are typically used and the photosensitivity can be enhanced by more than two orders of magnitude by hydrogen loading of the fiber prior to exposure.[14] Owing to the periodic nature of the index perturbation, only several discrete optical frequencies will resonate in the structure. Therefore, if broadband light is traveling in the core of the optical fiber the incident energy at such a resonant frequency will be reflected back down the optical fiber, with the remaining optical spectra unaffected, as illustrated in Fig. 1. The center wavelength of this resonance condition in an FBG is determined by the relationship:

$$\lambda_B = 2n_{eff}\lambda \tag{2}$$

where n_{eff} is the effective index of refraction of the core. The period can be adjusted by changing the relative angle of the two interfering UV beams, as seen by eqn (1), to create gratings with different Bragg wavelengths. Similarly, it can be seen that any change in the modulation spacing or overall refractive index will cause a

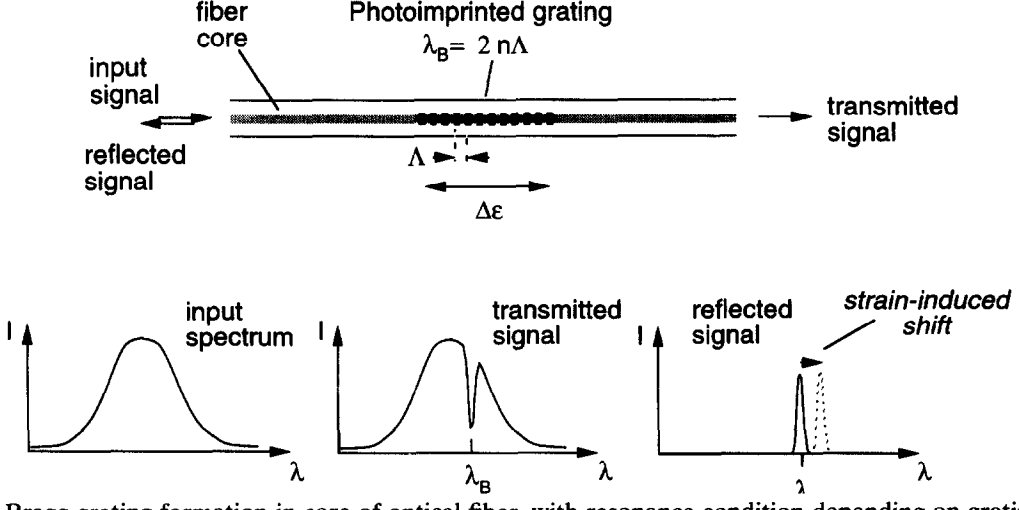

Fig. 1. Fiber Bragg grating formation in core of optical fiber, with resonance condition depending on grating spacing.

shift in the Bragg resonance wavelength. Consequently, any temperature- or strain-induced effects on the FBG can be determined by the corresponding shift in the center Bragg wavelength. If we look at strain-induced shifts only and assume isothermal conditions, the change in λ_B is given by:

$$\frac{\Delta\lambda_B}{\lambda_B} = (1-p_e)\epsilon \qquad (3)$$

where the strain over the length of the sensor is $\epsilon = \Delta L/L$, and p_e is the effective photoelastic constant for the fiber (approximately 0.22 for silica glass). From this equation the linear dependence of the device's reflected wavelength with applied strain is apparent. One major advantage of the FBG sensors is the ease with which several can be multiplexed along a single optical fiber. This can be accomplished by wavelength-division multiplexing (WDM) several FBG sensors, where each grating is written on the fiber with its Bragg resonance at different optical wavelengths as illustrated in Fig. 2. However, care must be taken to ensure that as the gratings are strained the reflected wavelengths from different gratings do not overlap,

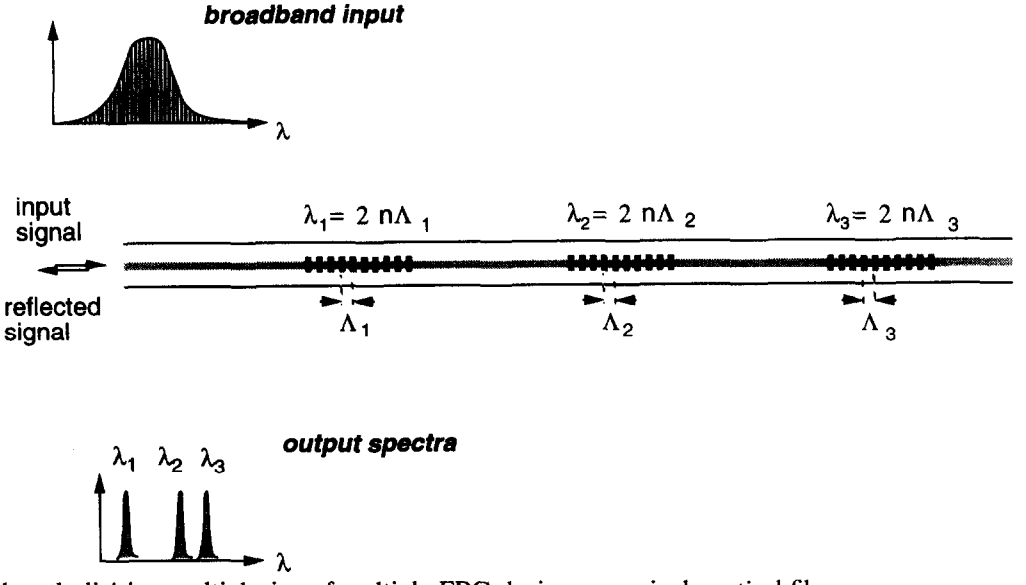

Fig. 2. Wavelength-division multiplexing of multiple FBG devices on a single optical fiber.

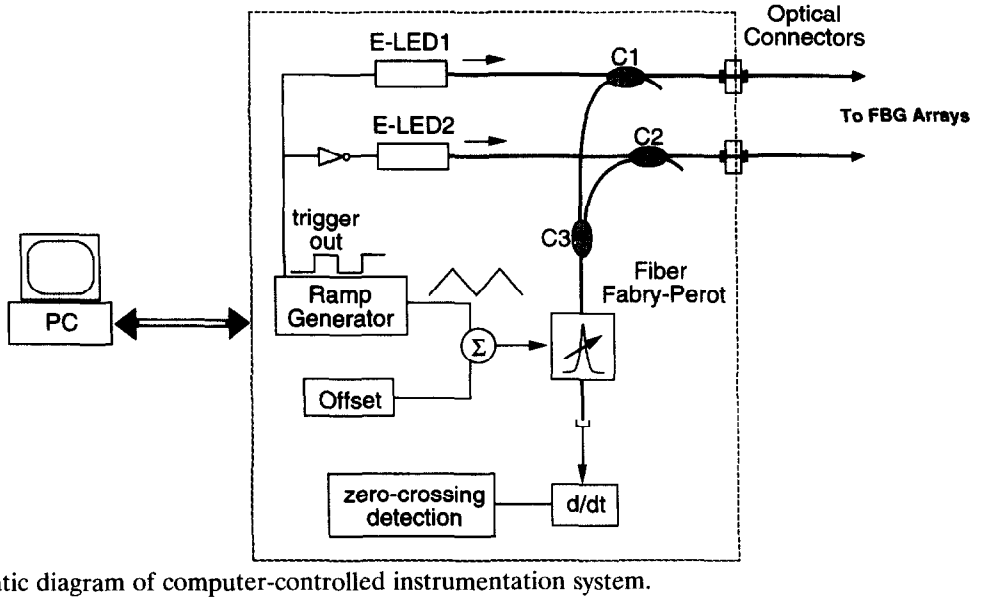

Fig. 3. Schematic diagram of computer-controlled instrumentation system.

and this requires the gratings to be spaced adequately to account for the maximum strain expected to be experienced by each device.

To track accurately the strain induced on the FBG sensors, the detection scheme must be able to detect very small wavelength shifts in the returned FBG signals. In the system presented here we use a fiber-optic tunable optical bandpass filter, the passband of which can be tuned through the application of a voltage to the device. The most straightforward technique using this filter would be to tune the filter until maximum power is passed, recording the applied voltage. A simple calibration between the applied voltage and the passband wavelength of the device will yield the returned wavelength from a sensor. One drawback of this device is the finite bandwidth of the passband, which is typically 0.3 nm; of the order of the spectral width of the FBG sensors. This finite width reduces the ability to determine precisely the peak reflected wavelength from the FBG sensor and therefore the resolution of the measurement. There are techniques to improve the resolution, one of which will be discussed later in this paper. Since the device is voltage-controlled it can be tuned to the wavelength returned by any of a number of WDM grating sensors. Therefore, simultaneous sensor readings may not be possible; however, with a fast

Fig. 4. Oscilloscope photograph from instrumentation system. Top trace: ramp applied to FFP filter; middle trace: derivative signals from FBG returned wavelengths; bottom trace: digital pulses sent to computer.

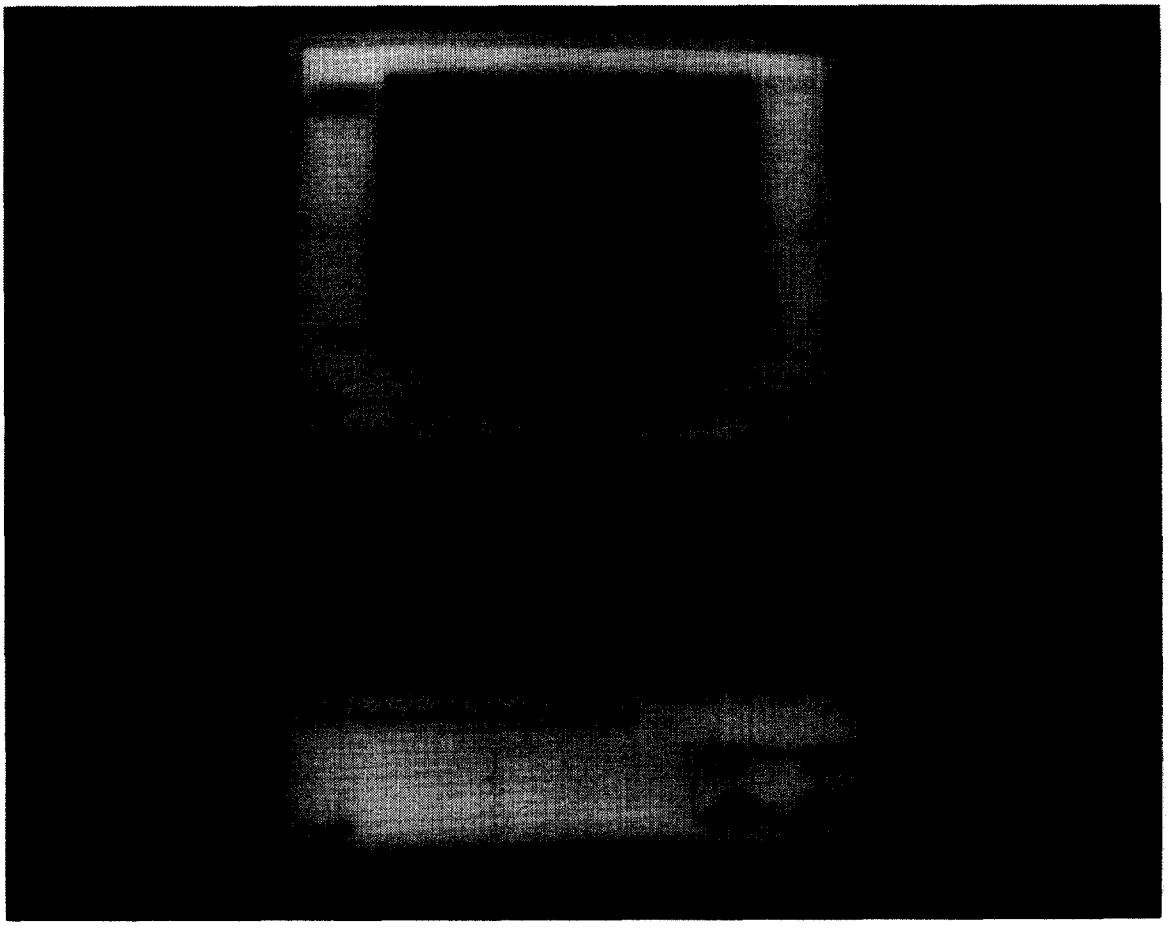

Fig. 5. Photograph of instrumentation system.

scanning voltage a high sampling rate can be achieved.

An additional restraint on the number of fiber Bragg grating sensors that can be interrogated in any system is the bandwidth of the optical source used to illuminate the devices. Leaving sufficient spacing between the nominal reflected wavelengths of the sensors to permit large strain readings without possible overlap would allow only a few sensors to be interrogated with a single source. However, there are several methods that can be used to expand the possible number of FBGs that can be interrogated, one of which is to use sequential addressing of different FBG arrays. The system we developed uses a hybrid time/wavelength multiplexing scheme to interrogate two arrays of FBG sensors; however, this number can easily be increased through the use of an optical switch, for example, to address possibly four, eight or 16 FBG arrays.

PROTOTYPE SYSTEM

The system we have developed to interrogate a number of wavelength-division multiplexed FBG sensors is shown schematically in Fig. 3. Light from two broadband sources (edge-emitting LEDs with 40 nm bandwidths, ELEDs) are

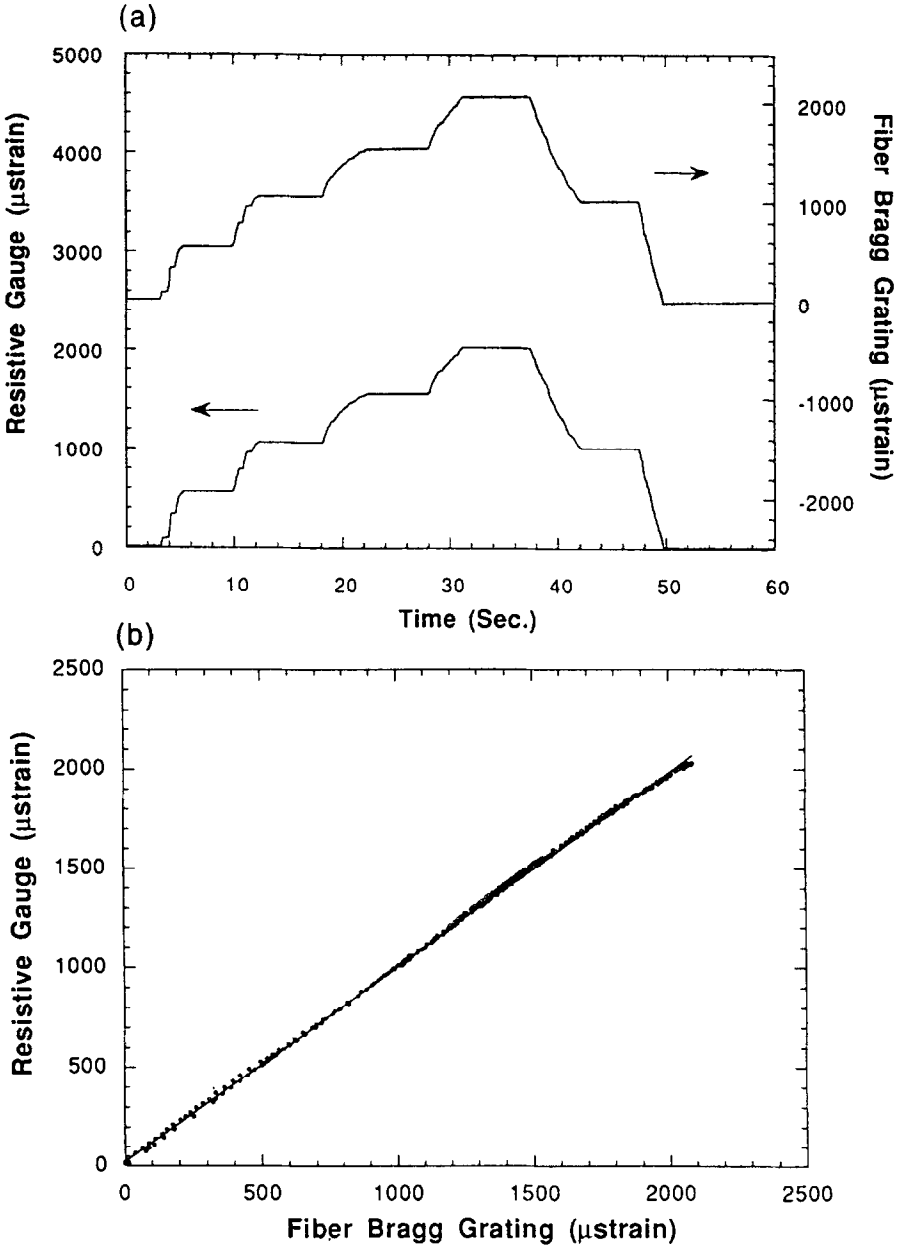

Fig. 6. (a) Strain response of FBG sensor and resistive gage; (b) correlation between FBG sensor and resistive gage.

sequentially directed through a pair of fiber-optic power-splitting fiber couplers (C1 and C2), where in each case half the power is guided to an optical connector and out to the array of FBG sensors. This connector permits the addressing of different arrays of FBGs by simply connecting to the array of interest. The reflected wavelength components of the FBG array travel back down the lead fiber and are directed, by way of couplers C1 and C2, to another coupler, C3, which recombines the returned signals and passes them to the input of a single-tunable FFP filter. This device acts as an optical narrow-bandpass filter with sufficient wavelength tuning range to encompass the reflected FBG wavelengths. A ramp waveform is applied to the FFP filter which sweeps the filter transmission window over the wavelength range occupied by the gratings. The two ELED sources are driven on/off synchronously with the ramp applied to the FFP filter, but in anti-phase with each other. Therefore only one set of returned signals from the two arrays of sensors pass through the FFP at any one time, since ELED1 is powered only during the up-scan in wavelength and ELED2 is powered during the down-scan. The output of the filter is then detected and, electronically, the derivative of the signal is obtained. This produces a series of derivative pulses for each of the signals reflected by the FBG sensors, with the zero-crossing of each pulse representing the peak reflected wavelength from each sensor, and permits improved resolution over simple peak detection for determination of the FBG reflected wavelengths. By referencing any shifts in the zero-crossings from each FBG sensor to the voltage applied to the filter, the strain at each FBG location can be obtained. The zero-crossing of the derivative signals are

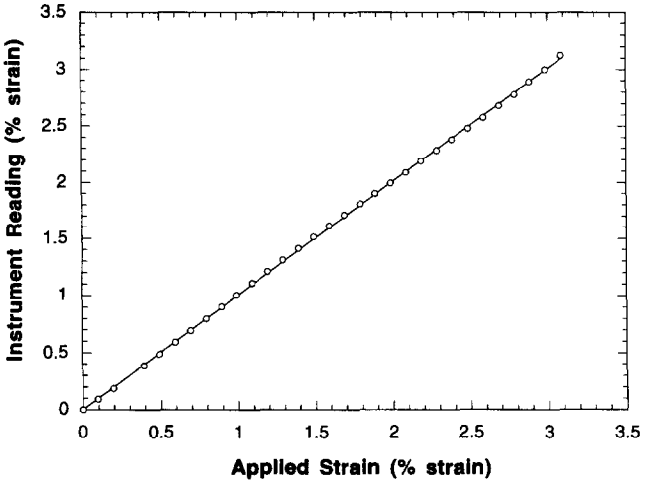

Fig. 7. Correlation between instrumentation system and strain applied to FBG sensor.

Table 1. FBG strain sensors embedded and tested in beams

Beam #	*# Gratings*	*Array/ Single*	*Comments*
8 ft #1	4	A and S	3-element array on rebar 1 element in FRP
8 ft #2	6	A (2)	two 3-element arrays on rebar
10 ft #1	5	A (2)	2-element array on rebar 3-element array in FRP
10 ft #2	5	A (2)	2-element array on rebar 3-element array in FRP
10 ft #3	4	A (2)	two 2-element arrays on rebar

Table 2. FBG strain sensors embedded and tested in deck panels

Beam #	*# Gratings*	*Array/ Single*	*Comments*
Deck #7	3	A and S	2-element array on rebar 1 element free float
Deck #8	4	A (2)	two 2-element arrays on rebar
Deck #11	3	A and S	2-element array on rebar 1 element free float
Deck #12	1	A	1 element on rebar

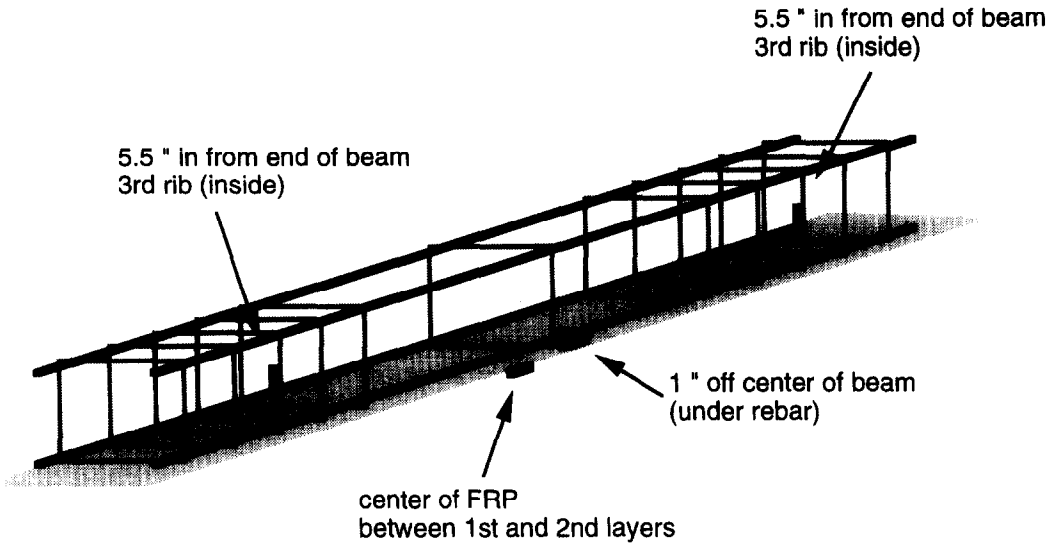

Fig. 8. Location of FBG sensors for 8 ft beam #1.

electronically turned into pulses and fed directly into a personal computer through the parallel port. This PC interface also permits software control of the scanning rate of the FFP filter (and therefore the sampling rate of the system): up to 150 Hz with a resolution of <1 μstrain. When started the program sets the sampling rate of the system and automatically determines the number of FBG sensors connected to the system. During data acquisition the strain values are displayed on-screen with a real-time graphical display and can also be optionally written to a disk for later use.

Figure 4 shows three oscilloscope traces which demonstrate the operation of the system. For testing purposes two arrays of FBGs were attached to the system, one array of four gratings and one array of five. The top trace in the photograph shows the ramp which is applied to the FFP filter. The second trace shows the derivative signals which are created for each FBG. On the up ramp the grating array of five sensors is illuminated as seen by the five pulses, while on the down ramp the array of four is illuminated. It is obvious in the photograph that the derivative pulses are of differing sizes, depending on the amplitude and shape of the returned signals from the FBG sensors. However, the system is insensitive to this effect as zero-crossings correspond to the wavelength returned by the devices. The bottom trace shows the pulses which are created from the derivatives and fed directly into the computer. Figure 5 shows a photograph taken of this prototype system with a lap-top computer used to control all functions of the box and for data acquisition.

CALIBRATION TEST

To test the accuracy of the system an FBG strain sensor was attached next to a conventional resistive strain gage (RSG) on a small aluminum plate. The plate was then subjected to three-point bending while strain readings were taken from both sensors. Figure 6(a) shows the results obtained as up to 2000 μstrain was applied to the plate. Good agreement can be seen between the two sensors, with the correlation plot in Fig. 6(b) demonstrating under 1% deviation between the two sensors. These devices have also been tested for high-strain applications as shown in Fig. 7. Here a strain of up to 3% was induced on a FBG sensor while data from the instrumentation system were recorded. Good linearity is shown between the two parameters.

EMBEDDED SENSOR TESTS

To test the performance of this system for internal monitoring of strains in concrete a number of arrays of gratings were embedded in rebar-reinforced concrete beams and deck panels. The structures were constructed at the Federal Highway Administration (FHWA) labs and were consequently loaded until failure while the internal strain was monitored. Fiber-reinforced plastic (FRP) composite layers were bonded to

the underside of the concrete beams to provide additional strengthening of the beam and several arrays of FBGs were also placed between layers of the composite. Table 1 lists the various FBG sensors which were embedded and tested. The two concrete beam sizes in which the sensors were embedded were 5 in × 8 in × 96 in and 9 in × 12 in × 120 in. Additionally, Table 2 lists FBG sensors which were embedded and tested in the concrete deck panels. These deck panels were 48 in × 99 in and 8 in thick. The bottom 3 in of each panel consisted of a prestressed concrete deck upon which a rebar matrix was laid and final concrete was poured. The sensors were attached to the rebar at approximately mid-height of the non-prestressed concrete section. Two sensors were also placed free floating just under the top surface of concrete (~1/8 in deep) in two of the deck panels.

In each case where the sensors were embedded in concrete the FBGs were bonded using typical foil gage adhesives (e.g. M-Bond 200) to a prepared section of rebar and coated with epoxy to protect the device. The lead fibers for each array of gratings were routed along the rebar elements and out the ends of the beams by way of small plugs attached to the concrete

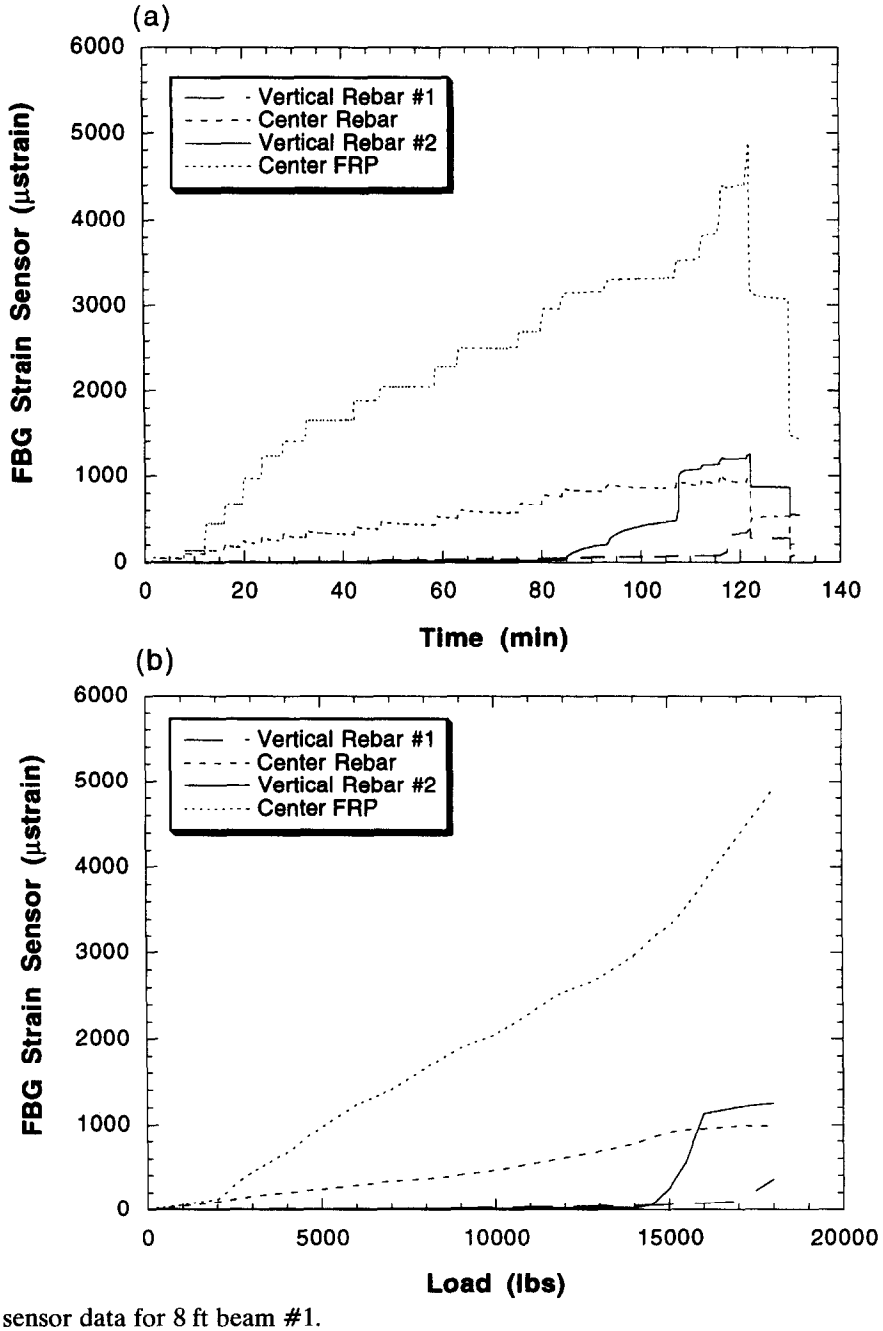

Fig. 9. FBG strain sensor data for 8 ft beam #1.

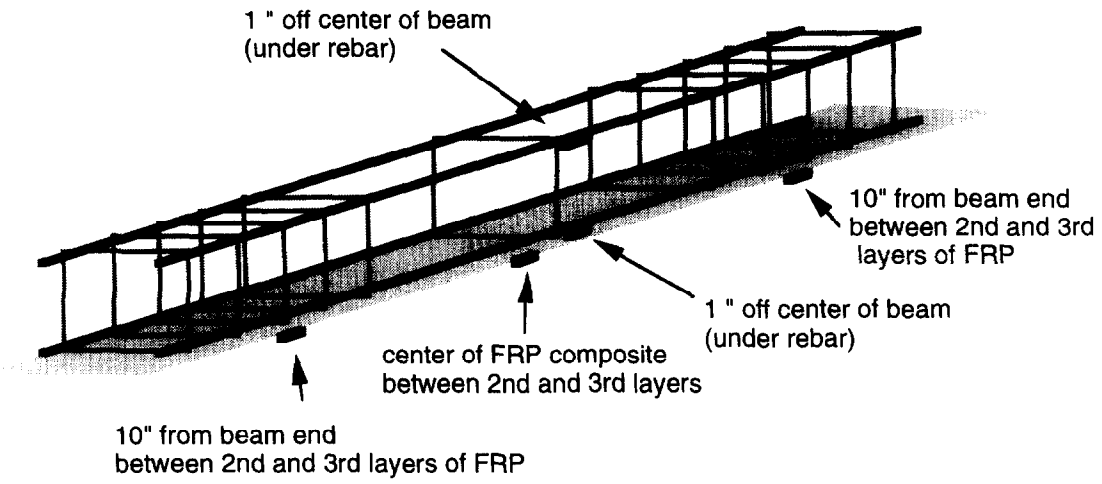

Fig. 10. Location of FBG sensors for 10 ft beam #1.

forms. This allowed access to the fibers once the concrete was set and the forms removed.

Figure 8 shows the FBG sensor placement along the rebar and in the FRP composite material for the first 8 ft beam. In this beam one array of three FBG sensors was attached to the rebar and embedded in concrete. The center FBG sensor was attached underneath one bottom rebar 1 in from the beam center. The two other sensors on the array were attached 5.5 in in from opposite ends of the beam on a vertical section of the rib rebars. Additionally, a single FBG element was placed between the first and second layers of FRP composite at the center point of the beam.

All the concrete beams were loaded in a four-point bending configuration until beam failure, which was defined as the point at which the beam could not sustain the applied load. In Fig. 9 the data for the 8 ft beam #1 up to the failure point at 18000 lbs are shown. The top trace shows the time record as the load was applied up to the final failure and the release of all loading after 130 min. The bottom trace shows the same data referenced to the load applied to the beam. As can be seen, the strain on the middle rebar and in the FRP material is well correlated up to about 2000 lbs load. At this point it is believed that the minor concrete cracking observed lessened the strength of the concrete–rebar section. With further applied load the FRP material is now supporting the beam as seen by the increasing strain observed by the FRP grating. The sudden jump in strain seen by one of the vertical FBG sensors at around 15000 lbs is attributed to a large crack that formed in the concrete through that rebar section. Consequently as the load is increased up to 18000 lbs the beam fails, with the failure point located at the end of the beam corresponding to the location of this FBG sensor.

In the first 10 ft beam the two arrays of sensors were placed as shown in Fig. 10. Here one array of two FBGs was attached to the rebar and embedded with one sensor placed on the under side of a top rebar and the other under a bottom rebar. The second array of three FBG elements was placed between the second and third layers of FRP material attached to the underside of the beam.

Figure 11 shows the data obtained as the beam was loaded. As before, the time trace is shown along with the same data plotted against the applied load. In this situation it is interesting to note the negative or compressive strain observed by the top rebar FBG sensor as the beam is loaded until failure at 47500 lbs, approximately 21 min into the test. The data also show that the center rebar and the FRP grating detected the most strain in the structure. It is also interesting to note the sharp increase in strain measured by one end FRP sensor starting at 25000 lbs. The location of this sensor again correlates with the end failure point of the beam as in the test previously described. All the sensors survived beam failure and after 27 min the load was released and residual strain detected as seen in the data. Figure 12 shows a photograph of this 10 ft beam loaded until failure in the four-point bending configuration. The failure region of this beam can be seen towards the right of the picture.

The data obtained for the other three reinforced concrete beams were similar to those for the two beams shown here. In each case the beams failed at one end with the composite

material breaking free of the main body of the beam. Additionally, as in the two cases presented, the general failure location was predicted in each case by a large increase in strain detected in the area prior to beam failure. This strain was detected along the rebar embedded in the concrete and/or in the FRP composite material. All sensors survived the embedding process, with only one fiber breakage occurring in the optical fiber interconnecting two FBG sensors. However, both sensors in this array were accessible from the two opposite ends of the optical fiber.

The four deck panels were similarly loaded until failure in a three-point loading configuration as shown in Fig. 13. Data taken during the loading of one of these deck panels (deck #7) are shown in Fig. 14. The three sensors embedded consisted of an array of two FBGs and one free-floating sensor. The two sensors of the array were attached to the rebar, one at the 1/4 point and the other at the 1/2 point along the length of the panel. The free-floating sensor was placed in the center of the deck, ~1/8 in from the top and embedded into the concrete. As can be seen from the data, initially all the

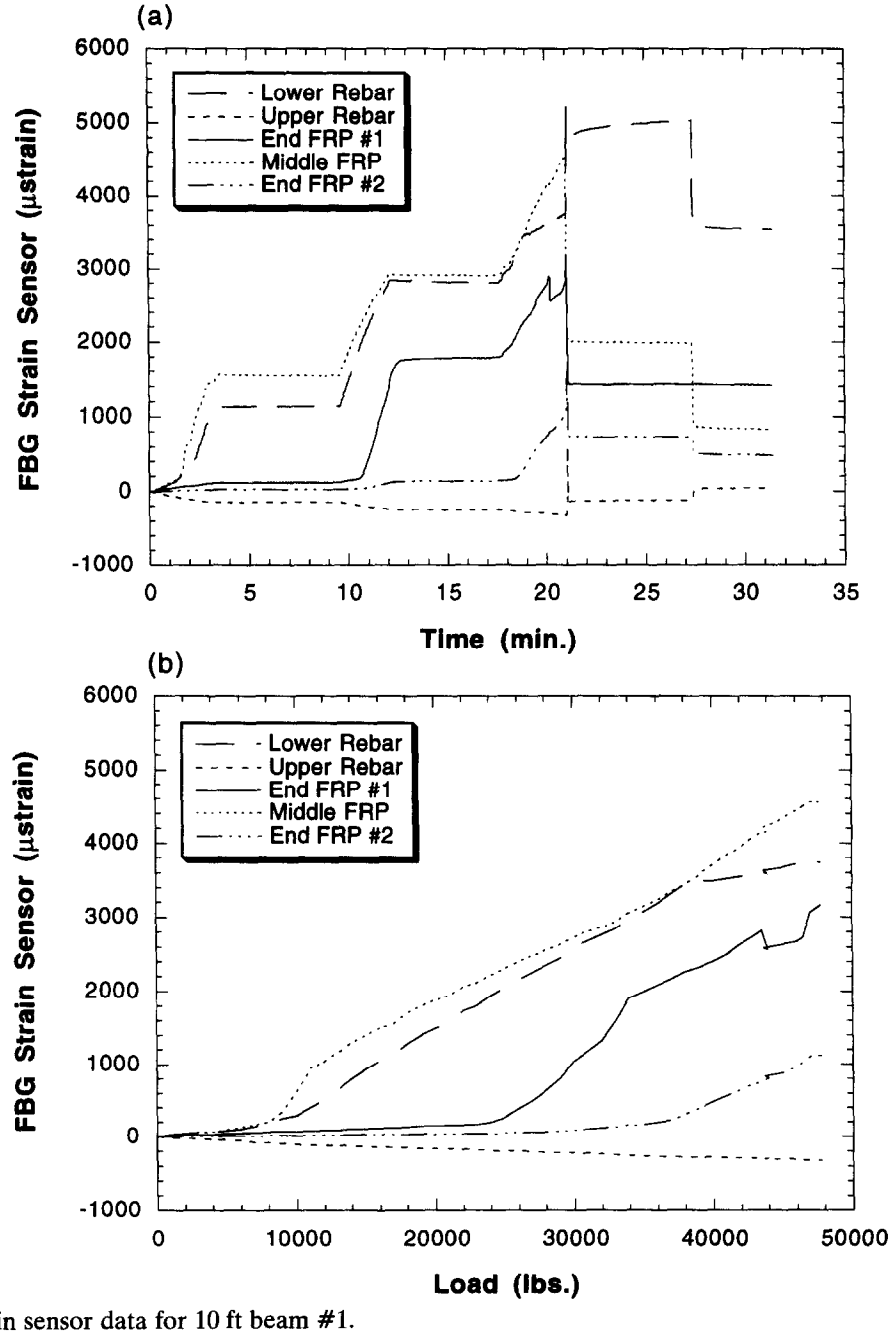

Fig. 11. FBG strain sensor data for 10 ft beam #1.

Fig. 12. Photograph of 10 ft beam #1 failure (shown in lower right side of beam).

sensors show compressive strains as the deck is loaded. As the applied load increases the neutral axis in the concrete moves up through the height of the deck panel, where the neutral

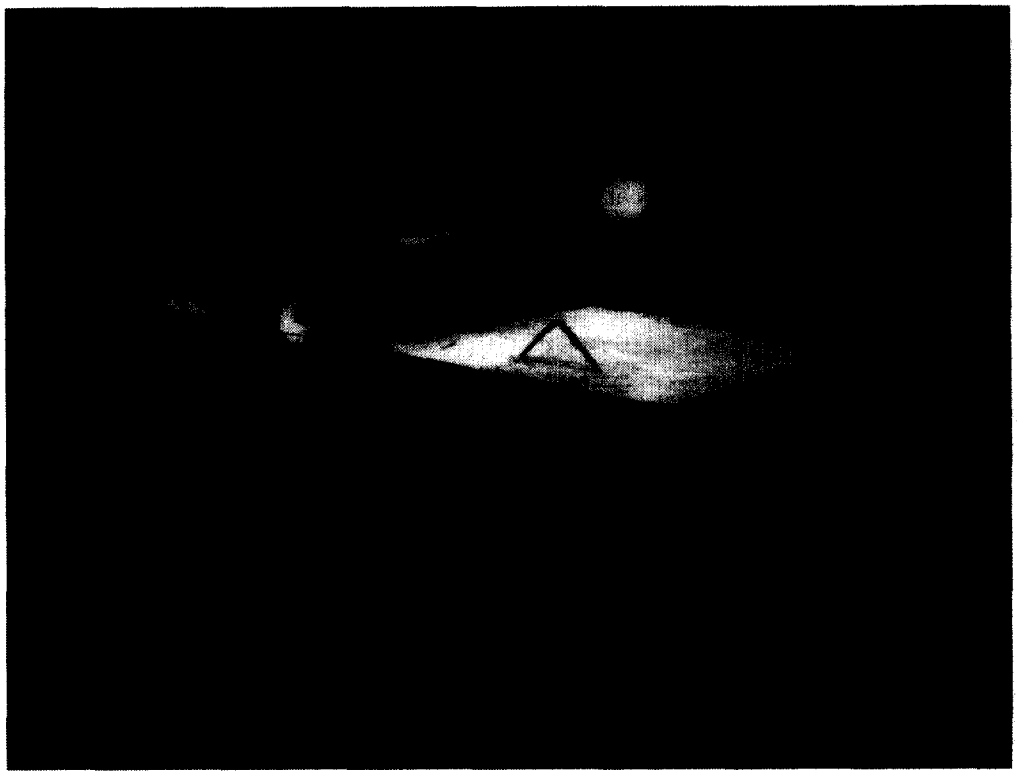

Fig. 13. Photograph of the three-point bending configuration for the deck panels.

axis is the point of no strain; above the axis there is compressive strain, below tensile. The movement of this axis can be seen in the data obtained from the two sensors attached to the rebar. Figure 14(b) shows an enlarged portion of the full data set obtained. Here it is seen that the center rebar FBG transitions from compressive to tensile strain at ~30000 lbs load. One would expect this sensor to respond to the movement of the neutral axis in the concrete first because of its location at the center of the panel, also the point of loading and maximum strain, relative to the unstrained ends of the panel. The neutral axis crosses over the 1/4 rebar sensor with an applied load of 40000 lbs. The panel failed at 48000 lbs with ~4000 μstrain observed by the free-floating FBG sensor and almost 3000 μstrain on the cen-

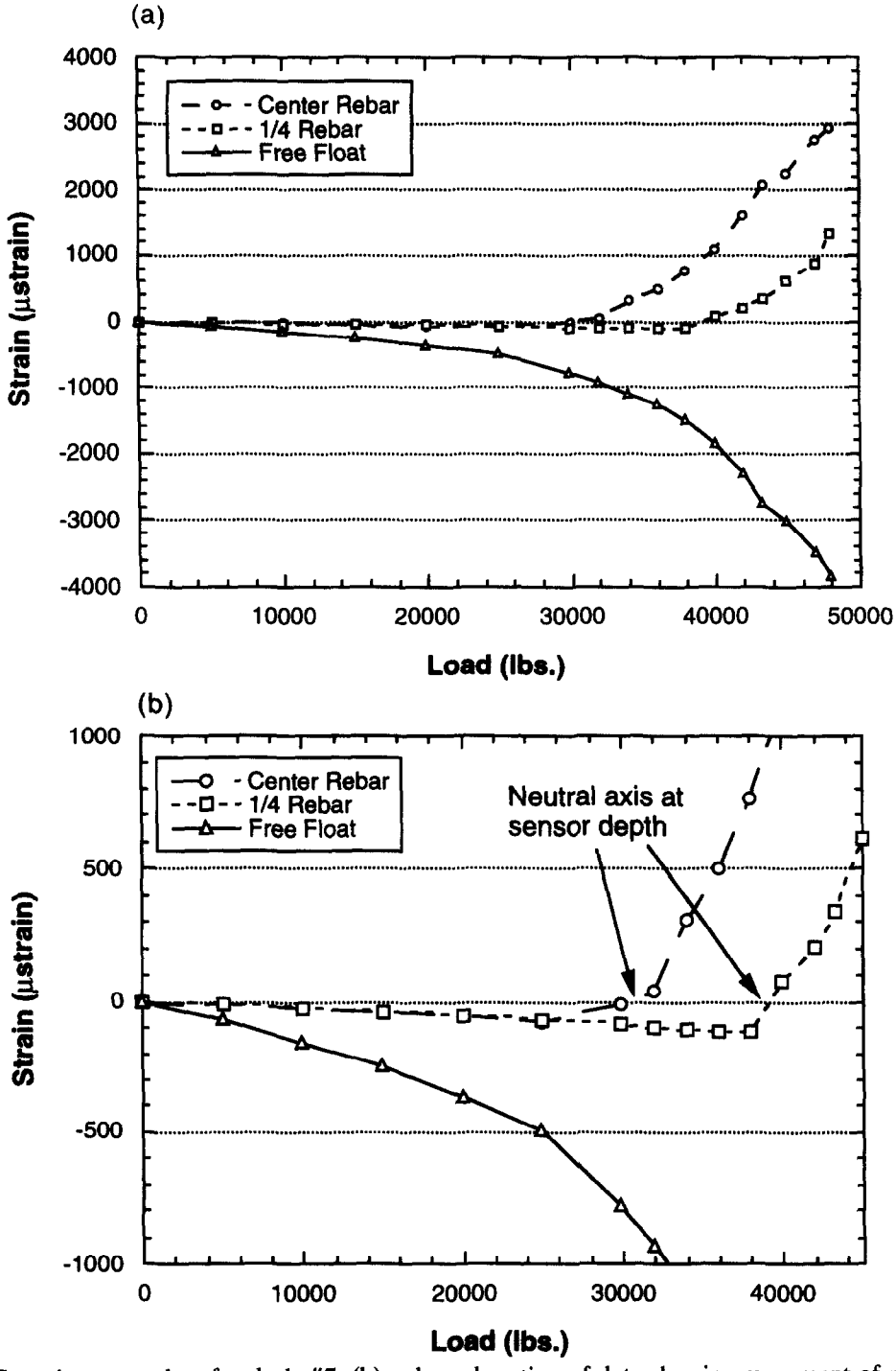

Fig. 14. (a) FBG strain sensor data for deck #7; (b) enlarged section of data showing movement of neutral axis through sensor locations.

ter rebar FBG sensor. The other three deck panels exhibited similar results as they were loaded.

SYSTEM IMPROVEMENTS

The capabilities of the system have been expanded since the onset of this work. By improving the scan rate and data acquisition the system can now sample at a rate of 287 Hz. With an optical switch attached to the system the total number of sensors that can be addressed has increased to 48, through the use of four arrays of 12 FBG sensors. The sampling rate of the system with the optical switch is then limited by the switching speed of that device. The system still maintains a resolution of ~ 1 μstrain with these improvements. We expect to test this system on a 1/4-scale bridge structure in the near future.

SUMMARY

We have reported the development of an interrogation system for FBG sensors and the installation and testing of the FBG sensors in concrete beams reinforced with FRP composite and prestressed deck panels. The instrumentation system developed is capable of addressing up to four arrays of four to 12 FBG sensors each, depending upon the maximum range of the sensors, which would be $\sim 10\,000$ μstrain for four sensors. The system is capable of ~ 1 μstrain resolution and sampling rates of up to 287 Hz. A computer interface to the instrumentation unit provided software control of the important parameters of the unit as well as data acquisition for real-time graphical display and data logging.

To date, 24 FBG sensors have been embedded and tested in concrete beams and 11 in deck panels. These devices were successfully used to measure the strain levels in the concrete structures as they were loaded to failure, in some cases demonstrating the potential of these devices to indicate the failure region in such structures. It should also be noted that all FBG sensors survived the full failure tests, with readings still being taken after beam failure occurred.

ACKNOWLEDGEMENTS

This work was sponsored by the Federal Highway Administration. We gratefully acknowledge Lloyd Cayes and Rick Kaiser for their help in constructing and testing the concrete structures.

REFERENCES

1. Mendez, A. & Morse, T. F., Overview of optical fiber sensors embedded in concrete. In *Proc. Fiber Optic Smart Structures and Skins V*, SPIE Vol. 1798, Boston, 1992.
2. Measures, R., Smart Structures: a revolution in civil engineering. In *Advanced Composite Materials in Bridges and Structures*. Canadian Society of Civil Engineering, Montreal, Quebec, 1992, p. 31.
3. Measures, R. M., Alavie, A. T., Maaskant, R., Ohn, M., Karr, S. & Huang, S., A structurally integrated Bragg grating laser sensing system for a carbon fiber prestressed concrete highway bridge. *Smart Mater. Struct.*, **4** (1995) 20.
4. Morey, W. W., Dunphy, J. R. & Meltz, G., Multiplexed fiber Bragg grating sensors. In *Proc. Distributed and Multiplexed Fiber Optic Sensors*, SPIE Vol. 1586. Boston, September 1991, paper #22.
5. Measures, R. M., Melle, S. M. & Liu, K., Wavelength demodulated Bragg grating fiber optic sensing systems for addressing smart structure critical issues. *Smart Mater. Struct.*, **1** (1992) 36.
6. Kersey, A. D., Berkoff, T. A. & Morey, W. W., High resolution fiber grating based strain sensor with interferometric wavelength shift detection. *Electronic Lett.*, **28** (1992) 236.
7. Kersey, A. D., Berkoff, T. A. & Morey, W. W., Fiber optic Bragg grating strain sensor with drift-compensated high-resolution interferometric wavelength shift detection. *Opt. Lett.*, **18** (1992) 72.
8. Kersey, A. D. & Morey, W. W., Multiplexed Bragg grating fibre-laser strain-sensor system with mode-locked interrogation. *Electronic Lett.*, **29** (1993) 112.
9. Kersey, A. D., Berkoff, T. A. & Morey, W. W., Multiplexed fiber Bragg grating strain-sensor system with a fiber Fabry–Perot wavelength filter. *Opt. Lett.*, **18**(16) (1993) 1370–1372.
10. Hill, K. O., Fujii, Y., Johnson, D. C. & Kawasaki, B. S., Photosensitivity in optical fiber waveguides: application to reflection filter fabrication. *Appl. Phys. Lett.*, **32** (1978) 647–649.
11. Meltz, G., Morey, M. M. & Glenn, W. H., Formation of Bragg gratings in optical fibers by a transverse holographic method. *Opt. Lett.*, **14** (1989) 823–825.
12. Askins, C. G., Putnam, M. A., Williams, G. M. & Friebele, E. J., Stepped-wavelength optical-fiber Bragg grating arrays fabricated in line on a draw tower. *Opt. Lett.*, **19**(2) (1994) 147.
13. Hill, K. O., Malo, B., Bilodeau, F., Johnson, D. C. & Albert, J., Bragg grating fabricated in monomode photosensitive optical fiber by UV exposure through a phase mask. *Appl. Phys. Lett.*, **62**(10) (1993) 1035.
14. Lemaire, P. J., Atkins, R. M., Mizrahi, V. & Reed, W. A., High pressure H_2 loading as a technique to achieving ultrahigh UV photosensensitivity and thermal sensitivity in GeO_2 doped optial fibres. *Electronic Lett.*, **29**(13) (1993) 1191.